Supplementary Information

Unlocking High-Voltage Sodium Ion Batteries with MOF-Derived Cr_2S_3@C Anode Materials

Mingqing Sun,[†,1] Zhiyuan Li,[†,1] Mei Yang,[*,†] Meng Xu,[†] Xiaoqing Chang,[†] Jianghua Wu,[‡] Liuqi Wang,[†] Xingyu Wang,[†] Tingting Chen,[†] Qiuying Xia,[*,†] and Hui Xia[*,†]

[†]School of Materials Science and Engineering, Nanjing University of Science and Technology, Nanjing 210094, China

[‡]National Laboratory of Solid State Microstructures, College of Engineering and Applied Sciences and Collaborative Innovation Center of Advanced Microstructures, Nanjing University, Nanjing 210093, China

[1]Both authors contributed equally to this work.

Corresponding Authors

E-mail: bayberry616@njust.edu.cn (M. Y.); qiuyingxia@njust.edu.cn (Q. X.); xiahui@njust.edu.cn (H. X.)

Negative-to-Positive (N/P) Capacity Ratio Used in the Full Cell Assembly

Base on the Cr_2S_3@C anode delivers an initial specific capacity of ~974 mAh g^{-1} at 0.1 A g^{-1} (ICE=78.4%), while the $Na_3V_2(PO_4)_3$ cathode provides an initial specific capacity of ~100 mAh g^{-1} (ICE=95%). Full cell assembles employed mass loadings (1.1 mg for the anode and 7.6 mg for the cathode), the resulting N/P ratio is ~1.16, calculated as: (anode specific capacity × ICE × anode mass loading) / (cathode specific capacity × ICE × cathode mass loading) = (974 mAh g^{-1} × 0.784 × 1.1 mg) / (100 mAh g^{-1}×0.95 × 7.6 mg). (While 974 mAh g^{-1} and 100 mAh g^{-1} represents the specific capacity of Cr_2S_3@C and $Na_3V_2(PO_4)_3$. 0.784 and 0.95 represents the ICE of Cr_2S_3@C and $Na_3V_2(PO_4)_3$. 1.1 mg and 7.6 mg represents the mass loading of Cr_2S_3@C and $Na_3V_2(PO_4)_3$).

Energy density = Specific capacity (total mass basis) × Average voltage. Then, the energy density calculation is: 86 mAh g^{-1} × 2.4 V = 206 Wh kg^{-1}, where 86 mAh g^{-1} represents the specific capacity based on the combined mass of Cr_2S_3@C anode and $Na_3V_2(PO_4)_3$ cathode.

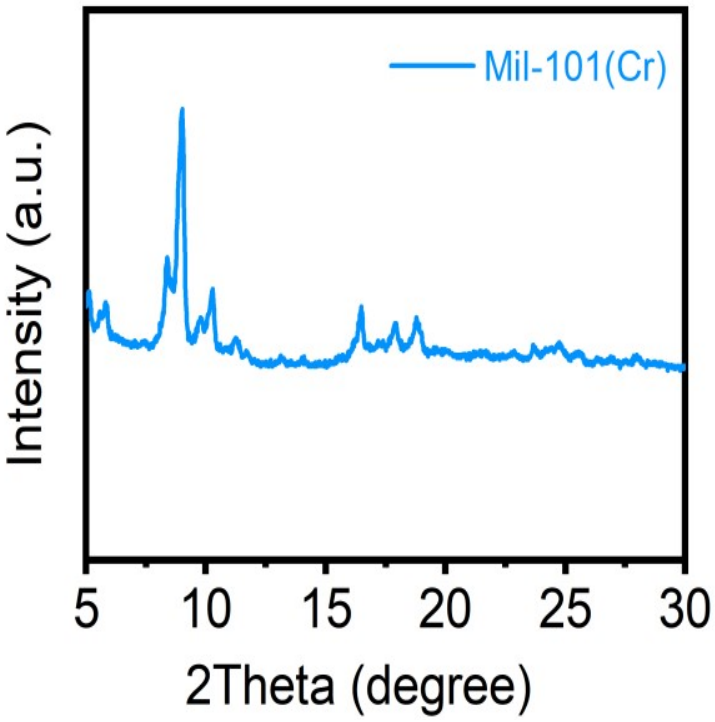

Fig. S1 XRD pattern of MIL-101(Cr) MOF precursor.

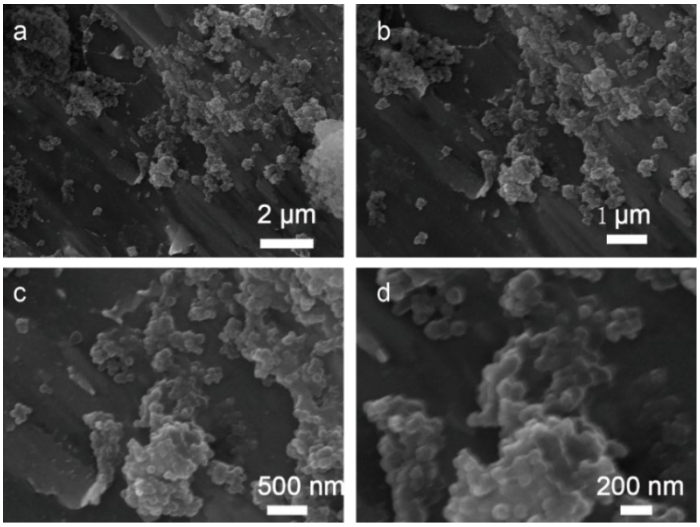

Fig. S2 SEM images of the MIL-101(Cr) MOF precursor.

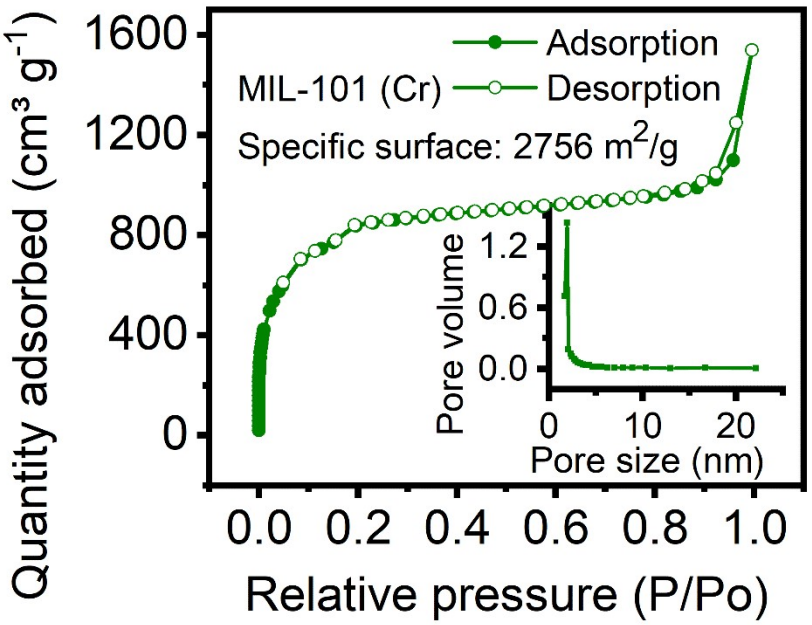

Fig. S3 Nitrogen adsorption-desorption isotherms, with an inset detailing the pore size distribution of MIL-101(Cr) MOF precursor.

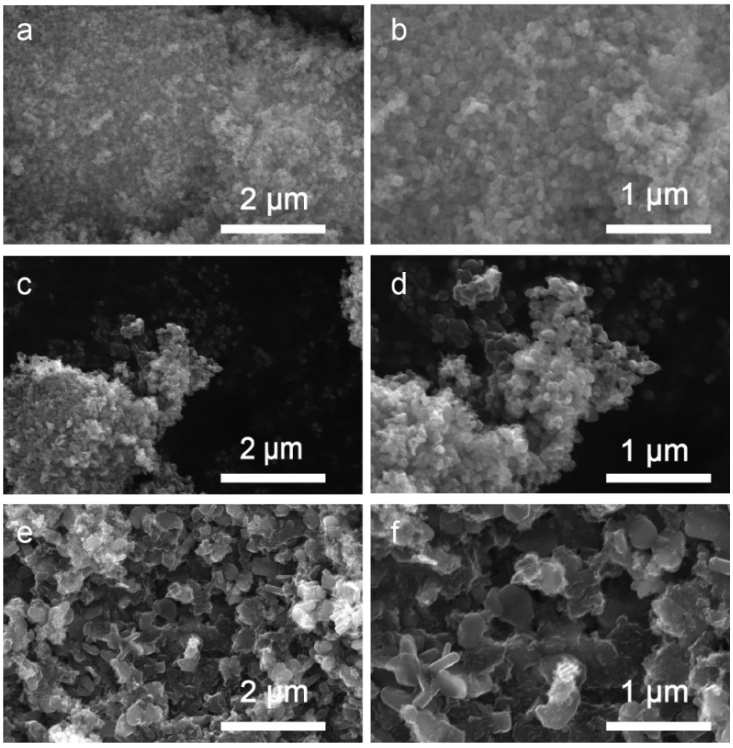

Fig. S4 Morphological characterization of Cr_2S_3@C samples at different temperatures (a,b) Cr_2S_3@C-700, (c,d) Cr_2S_3@C-800 (denoted as Cr_2S_3@C), and (e,f) Cr_2S_3@C-900.

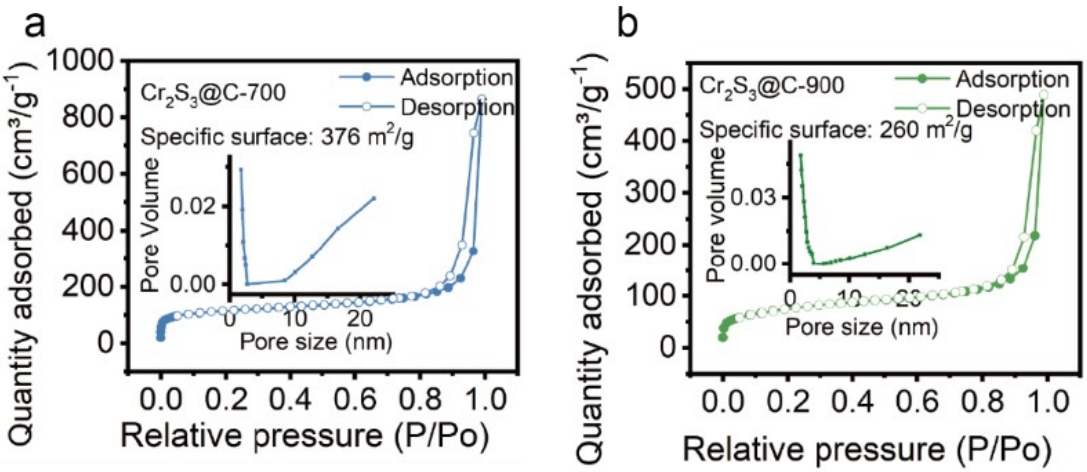

Fig. S5 Nitrogen adsorption-desorption isotherms, with an inset detailing the pore size distribution of (a) Cr_2S_3@C-700 and (b) Cr_2S_3@C-900.

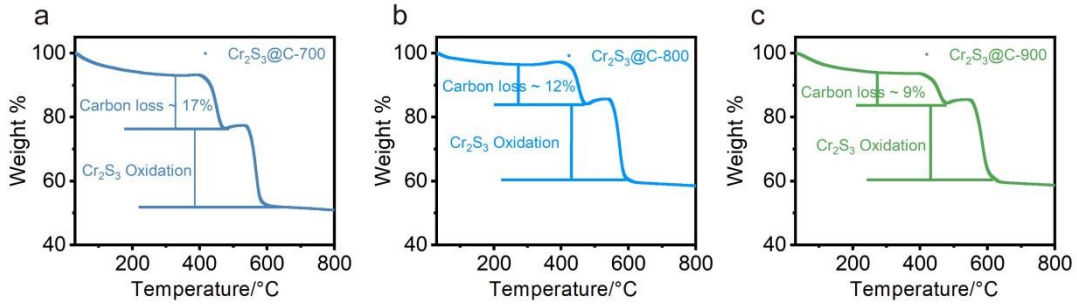

Fig. S6 TGA curves of (a,b) Cr_2S_3@C-700, (c,d) Cr_2S_3@C and (e,f) Cr_2S_3@C-900

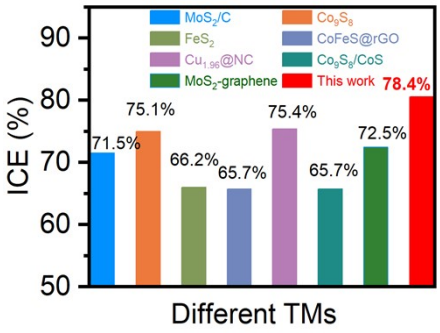

Fig. S7 A comparison of the Initial Coulombic efficiency (ICE) for representative transition-metal sulfide (TMS) anodes in sodium-ion batteries. The data sources (Refs. [1–7]) are provided below.[1–7]

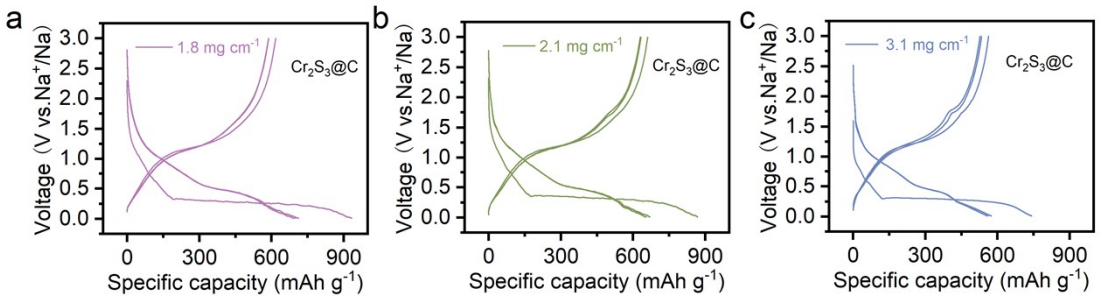

Fig. S8 Galvanostatic charge-discharge curves of Cr_2S_3@C electrodes with different mass loadings: (a) 1.8 mg cm^{-2}, (b) 2.1 mg cm^{-2}, and (c) 3.1 mg cm^{-2} at 0.1 A g^{-1}.

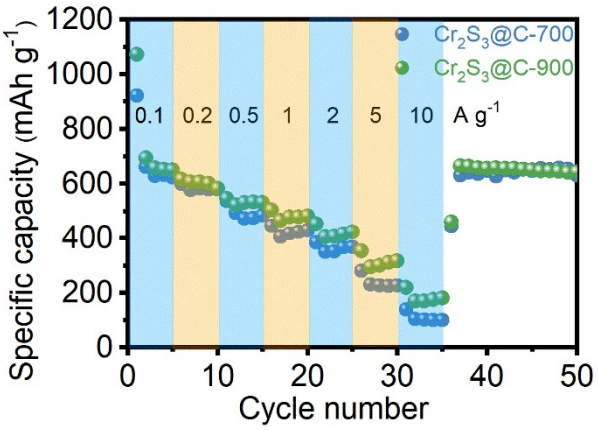

Fig. S9 (a) Rate performance of Cr_2S_3@C-700 and Cr_2S_3@C-900.

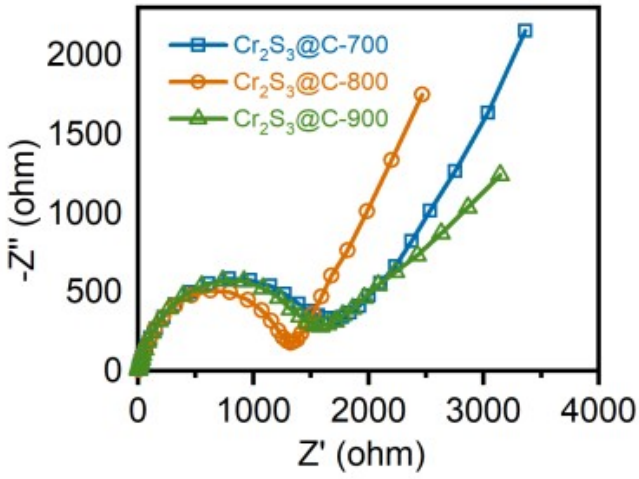

Fig. S10 Nyquist plots of Cr_2S_3@C-700, Cr_2S_3@C, and Cr_2S_3@C.

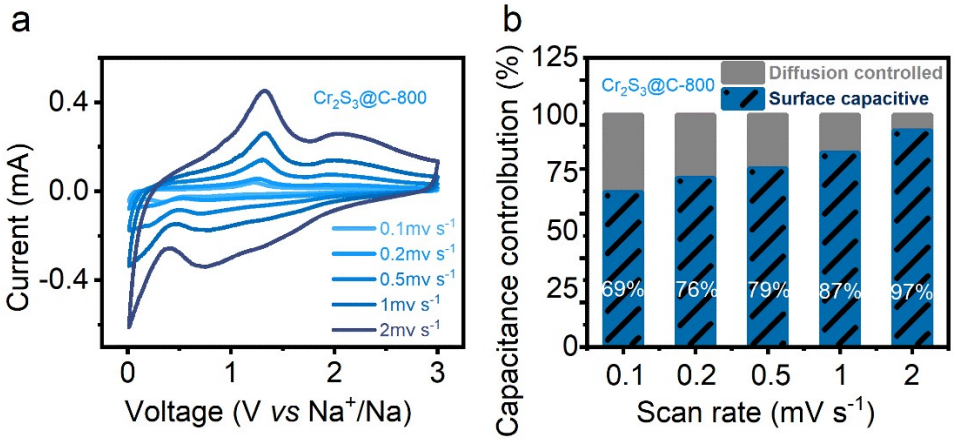

Fig. S11 (a) CV curves of the Cr_2S_3@C at different scan rates. (b) Pseudocapacitive contribution at different scan rates.

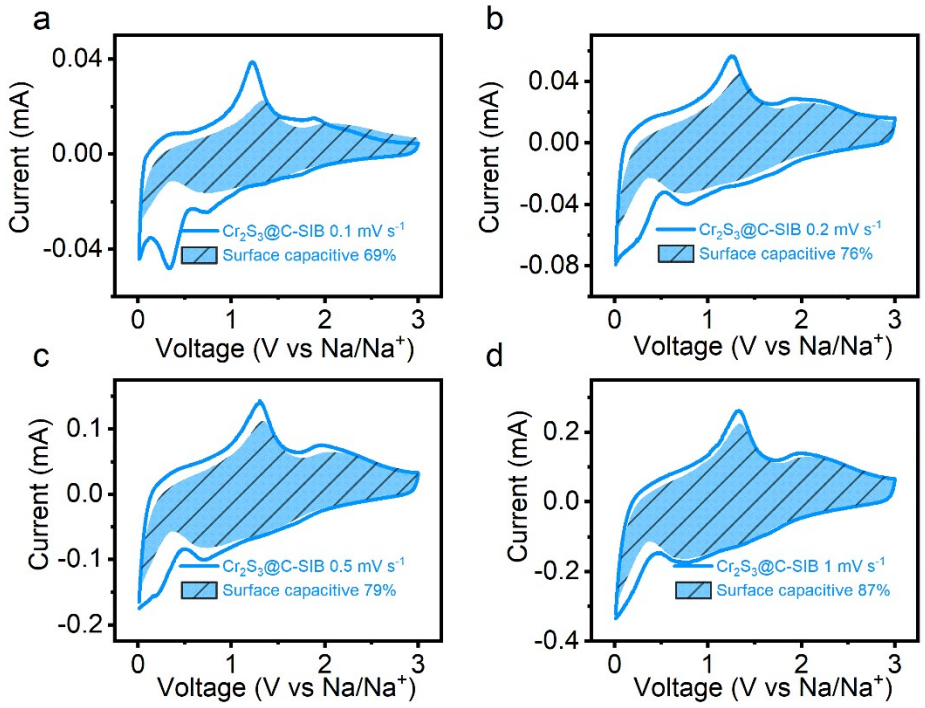

Fig. S12 CV curves of the Cr_2S_3@C electrode in Na-ion batteries at different scan rates of 0.1, 0.2, 0.5, and 1 mV s^{-1}, with the pseudocapacitive contribution shown by the blue area.

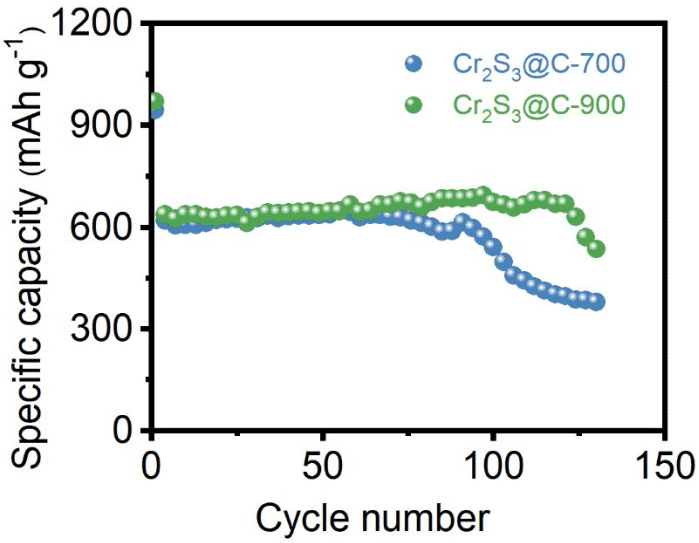

Fig. S13 Long-term cycling performance of Cr_2S_3@C-700 and Cr_2S_3@C-900 at 0.2 A g^{-1}.

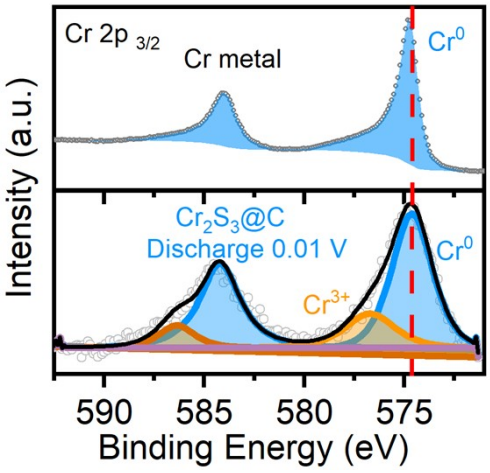

Fig. S14 Cr 2p XPS spectra of metallic Cr reference and discharged Cr_2S_3@C electrode (0.01 V).

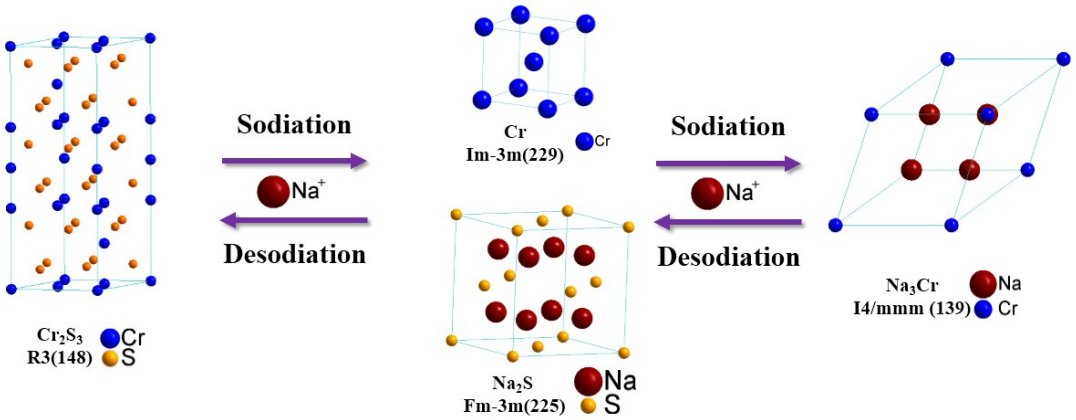

Fig. S15 The reaction mechanism of Cr_2S_3@C in sodium-ion batteries.

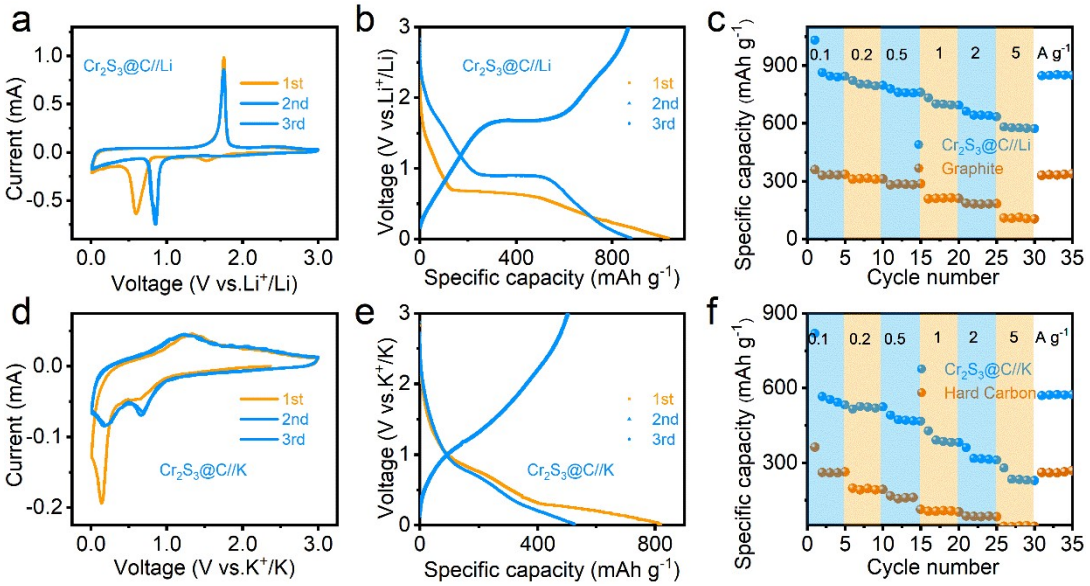

Fig. S16 (a,d) CV profiles of the Cr_2S_3@C anode at scan rate of 0.1 mV s^{-1}, and (b,e) GCD profiles at 0.1 A g^{-1} for the initial 3 cycles (c,f) Rate performance in both lithium-ion batteries (LIBs) and potassium-ion batteries (KIBs), respectively.

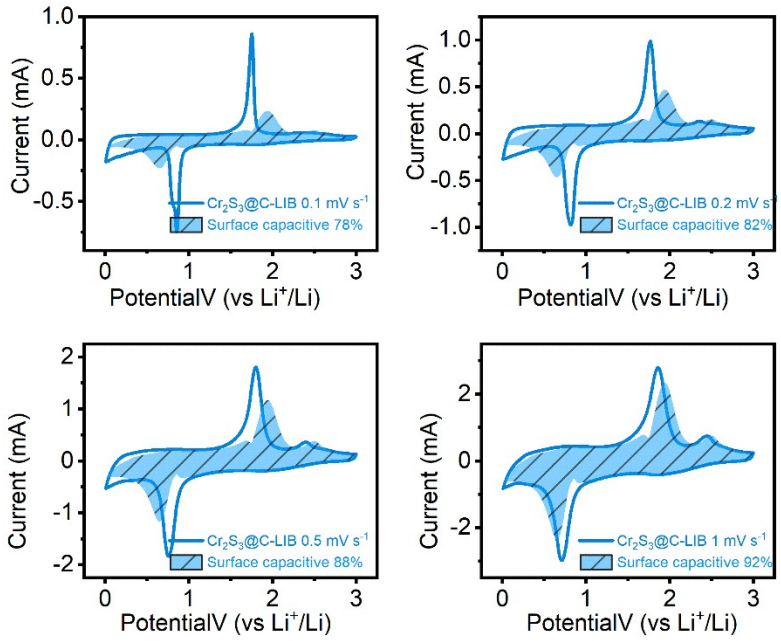

Fig. S17 CV analysis of Cr_2S_3@C in a LIB half cell. CV curves at different scan rates of 0.1, 0.2, 0.5, and 1 mV s^{-1}, with the pseudocapacitive contribution highlighted by the blue area.

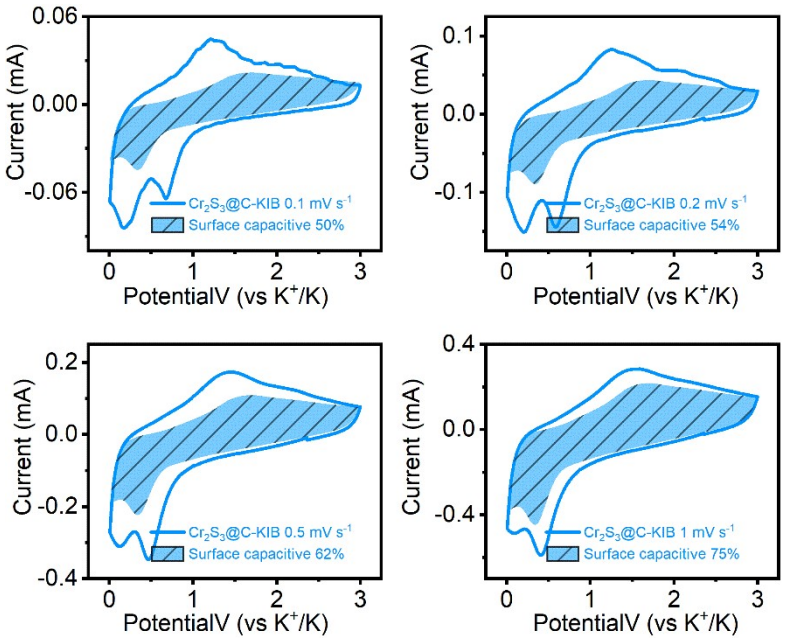

Fig. S18 CV analysis of Cr_2S_3@C in a KIB half cell. CV curves at different scan rates of 0.1, 0.2, 0.5, and 1 mV s^{-1}, with the pseudocapacitive contribution highlighted by the blue area.

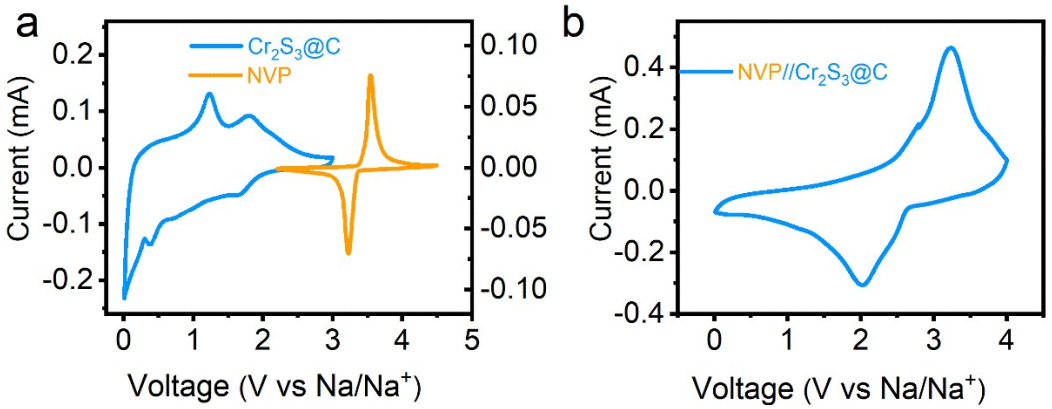

Fig. S19 (a) CV profiles of the NVP cathode and Cr_2S_3@C anode in separate sodium-ion half cells. (b) CV profiles of the NVP//Cr_2S_3@C in the sodium-ion full cell.

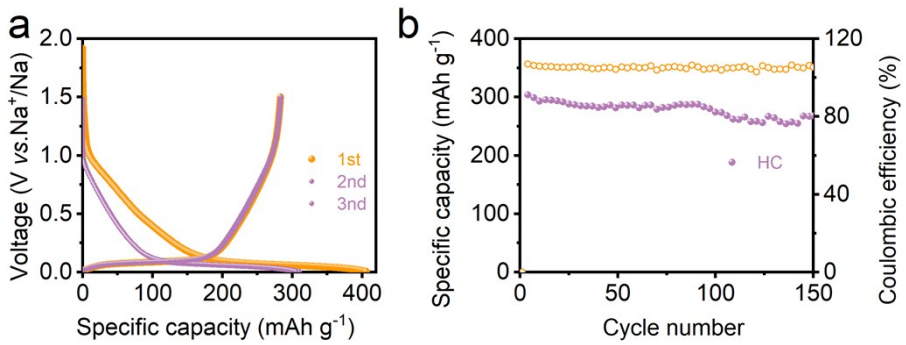

Fig. S20 (a) GCD profiles of the hard carbon (HC) anode for the initial 3 cycles at 0.02 A g^{-1} (b) Long cycle performance of the HC anode at 0.02 A g^{-1}.

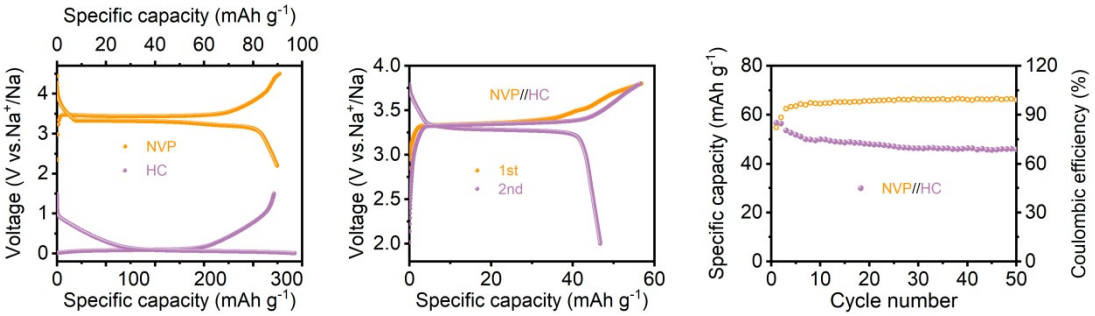

Fig. S21 (a) GCD profiles of the NVP cathode and Cr_2S_3@C anode for the initial 3 cycles at 0.02 A g^{-1}; (b) GCD profiles and (c) cycle performance of the NVP//Cr_2S_3@C full cell.

Table S1 Comparison of the specific surface area of Cr_2S_3@C in this study with those of other TMS composites reported for SIBs.[8–15]

Anode material	Specific surface area (m^2/g)	Reference
In_2S_3@GO	55.79	ACS Applied Materials Interfaces 2017, 9 (28), 23723–23730.
NiS_2@C@C	25.7	Advanced Functional Materials 2018, 28 (41), 1803690.
MNS@NC	21.76	Small 2024, 20 (18), 2308136.
Sb-CuS@C	36.18	ChemSusChem, 202401271.
CoS_2@C	55.9	Small 2018, 14 (41), 1802716.
Cu_2SnS nano ball	44.8	ACS Applied Materials Interfaces 2017, 9 (31), 26038–26044.
SnS@NC	75	Angewandte Chemie International Edition 2019, 58 (3), 760–763.
SnS@CNT	44.3	Journal of Materials Science 2022, 57 (11), 6308–6319.
Cr_2S_3@C	321	This work

References:

1 S. H. Choi, Y. N. Ko, J. Lee and Y. C. Kang, *Advanced Functional Materials*, 2015, **25**, 1780–1788.

2 H. Peng, W. Miao, S. Cui, Z. Liu, B. Tao, W. Hou, G. Ma and Z. Lei, *Small*, 2024, **20**, 2404957.

3 G. Li, D. Luo, X. Wang, M. H. Seo, S. Hemmati, A. Yu and Z. Chen, *Advanced Functional Materials*, 2017, **27**, 1702562.

4 T. Zeng, Q. Chen, Y. Ding, X. Xu, D. Feng and D. Xie, *Journal of Energy Storage*, 2024, **76**, 109849.

5 D. Xie, X. Xia, Y. Wang, D. Wang, Y. Zhong, W. Tang, X. Wang and J. Tu, *Chemistry – A European Journal*, 2016, **22**, 11617–11623.

6 S. Huang, S. Fan, L. Xie, Q. Wu, D. Kong, Y. Wang, Y. V. Lim, M. Ding, Y. Shang, S. Chen and H. Y. Yang, *Advanced Energy Materials*, 2019, **9**, 1901584.

7 W. Ren, H. Zhang, C. Guan and C. Cheng, *Advanced Functional Materials*, 2017, **27**, 1702116.

8 X. Zheng, Z. Zhang, Z. Li, C. Shi, J. Zhao and J. Tang, *ChemSusChem*, 2025, **18**, e202401271.

9 C. Wang, H. Tian, J. Jiang, T. Zhou, Q. Zeng, X. He, P. Huang and Y. Yao, *ACS Applied Materials Interfaces*, 2017, **9**, 26038–26044.

10 X. Wang, J.-Y. Hwang, S.-T. Myung, J. Hassoun and Y.-K. Sun, *ACS Applied Materials Interfaces*, 2017, **9**, 23723–23730.

11 S. Wang, Y. Fang, X. Wang and X. W. (David) Lou, *Angewandte Chemie International Edition*, 2019, **58**, 760–763.

12 H. Zhu, Q. Liu, S. Cao, H. Chen and Y. Liu, *Small*, 2024, **20**, 2308136.

13 G. Zhao, Y. Zhang, L. Yang, Y. Jiang, Y. Zhang, W. Hong, Y. Tian, H. Zhao, J. Hu, L. Zhou, H. Hou, X. Ji and L. Mai, *Advanced Functional Materials*, 2018, **28**, 1803690.

14 L. Shi, D. Li, P. Yao, J. Yu, C. Li, B. Yang, C. Zhu and J. Xu, *Small*, 2018, **14**, 1802716.

15 H. Ding, Y. Wu, Y. Xia, T. Yang, Z. Hu, Q. Chen and G. Yue, *Journal of Materials Science*, 2022, **57**, 6308–6319.